IEEE Access
Multidisciplinary | Rapid Review | Open Access Journal

Received June 27, 2020, accepted July 5, 2020, date of publication July 10, 2020, date of current version July 22, 2020.

Digital Object Identifier 10.1109/ACCESS.2020.3008419

Study of the Ability of an Electromagnetic Flowmeter Based on Step Excitation to Overcome Slurry Noise

BIN LI[1], YUE YAN[1], JIE CHEN[1], AND XINGHANG FAN[1]
School of Mechatronic Engineering and Automation, Shanghai University, Shanghai 200444, China
Corresponding author: Jie Chen (jane.chen@shu.edu.cn)

ABSTRACT An electromagnetic flowmeter (EMF) can be used to measure the speed of slurry fluid. In this paper, according to Maxwell's equations and the dB/dt vortex electric field, a step excitation scheme is proposed. The original excitation process of the primary excitation current rise time is divided into a two-step excitation process. Without increasing the excitation current rise time, the equivalent excitation frequency is increased by increasing the primary *dB/dt*. This method can enhance the EMF's ability to overcome slurry noise. The paper analyzes the design parameters of the step excitation scheme and designs the software and hardware. After that, the paper compares the step excitation scheme with the three-value rectangular wave excitation scheme based on wavelet transform signal processing. Experiments show that the step excitation EMF has a lower steady-state fluctuation rate when measuring mortar and has a stronger ability to overcome slurry noise. Additionally, the step excitation EMF and Yokogawa AXF 040G EMF are compared experimentally. Through flow calibration, clean water measurement, mortar measurement and dynamic response experiment, it is verified that the step excitation EMF has the ability to enhance the resistance to slurry noise at the same excitation frequency.

INDEX TERMS Electromagnetic flowmeter, slurry noise, Maxwell's equations, step excitation, slurry noise overcoming method.

I. INTRODUCTION

Electromagnetic flowmeter (EMF) is widely used in modern industrial production. It is not easy for an EMF to become blocked because there are no movable parts and throttling parts in the pipe. In principle, it is suitable for measuring slurry-type fluids. An EMF will be affected by slurry noise [1] when measuring slurry. Slurry noise is the random noise produced by solid particles colliding with the electrode, which has the basic 1/f characteristic [2], [3] in the frequency spectrum; therefore, it has the following two characteristics.

First, in the time domain, the level of slurry noise generated on the electrode is jumping. The slurry noise is not fixed polarity interference, and the new charge generated in the fluid will continuously change the level of slurry noise interference on the electrode. Second, when the sand-to-water quality ratio of the mortar is fixed, the meaning time of the interference caused by the solid particles in the fluid colliding with the electrode is fixed. The smaller the value of unit time t is, the smaller the probability of new solid particles colliding with the electrode during this time, which reduces the probability of generating slurry noise.

Currently, improved excitation technology or improved software processing algorithms are commonly used to enhance an EMF's ability to overcome slurry noise.

In terms of signal processing, Evren Eryurek *et al.* proposed the wavelet processing method for a single-frequency rectangular wave excitation EMF [4]. Michael A. Linnert *et al.* designed the Kalman filter based on the state space model of EMF sensors [5]. Based on this algorithm, an EMF achieves lower energy consumption and higher accuracy. L. P. Liang *et al.* proposed the stationary wavelet transform (SWT) method to separate nonstationary slurry noise from flow signals [6] and improved the effect of suppressing slurry noise. A Sophian *et al.* proposed a new feature extraction method for pulsed eddy current in non-destructive testing, which realized the effective classification of defects [7]. By extracting the principal components

The associate editor coordinating the review of this manuscript and approving it for publication was Yassine Maleh.

with the highest variances, the effect of noise was reduced. This method provided a new idea for EMF signal processing.

In terms of the excitation mode, there is no polarization problem when measuring liquid metal [8], and DC excitation can be adopted. There are polarization problems when measuring electrolytes. Positive and negative square wave excitations are now commonly used, including two-value wave excitation, three-value wave excitation, and dual-frequency excitation [9]. These excitation methods include the excitation switching process and the constant excitation process.

In terms of the excitation frequency, the higher the EMF excitation frequency is, the stronger the ability to overcome slurry noise, which is the consensus of the EMF industry. Toshiba company proposed a dual-frequency excitation EMF [10] in which when the flow signal is relatively stable, the first excitation unit with an excitation frequency of 4.00 Hz to 8.00 Hz will be opened. When the slurry noise is large, the second excitation unit with an excitation frequency of 25.00 Hz to 35.00 Hz will be opened. ABB proposed improved AC excitation technology that increases the excitation frequency to 70.00 Hz and enhances the ability to suppress slurry noise [11], [12]. Japan's Yokogawa company proposed a dual-frequency excitation EMF with an excitation frequency of 75.00 Hz. To measure high-concentration slurry, 160.00 Hz enhanced EMF products were introduced [13].

Through previous analysis, at present, an EMF mainly improves the ability to overcome slurry noise by improving the excitation frequency. In this paper, the mechanism of overcoming slurry noise by high-frequency excitation is studied by analyzing the EMF excitation process. Under the guidance of this mechanism, this paper proposes a step excitation technology, which improves the excitation scheme, improves the equivalent excitation frequency without increasing the rise time of the excitation current, and improves the ability of an EMF to overcome slurry noise. The paper introduces the system design of the step excitation scheme.

II. ELECTRODE SIGNAL AND EXCITATION FREQUENCY CHARACTERISTICS UNDER POSITIVE AND NEGATIVE SQUARE WAVE EXCITATION CHARACTERISTICS

Faraday's law of electromagnetic induction has a wide range of applications [14]–[16]. An EMF is an instrument developed based on this law to measure the flow of conductive liquid. Fig. 1 is the basic structure diagram of an EMF measurement system. The excitation current generates a magnetic field through the coil. Fluid with the average velocity $\bar{v}$ cuts magnetic field line B to produce the induced electromotive force e_i, and $e_i = kBD\bar{v}$, where k is the constant and D is the inner diameter of the measuring pipe. At present, many EMFs use high excitation frequencies to overcome slurry noise, and the principle is very clear. Figs. 2 (a)-(c) are three commonly used positive and negative square wave excitation methods. These excitation methods all have two processes of excitation switching and constant excitation, as shown in Fig. 2 (d). The electromagnetic characteristics in both processes can be illustrated by Faraday's law of electromagnetic induction [19]

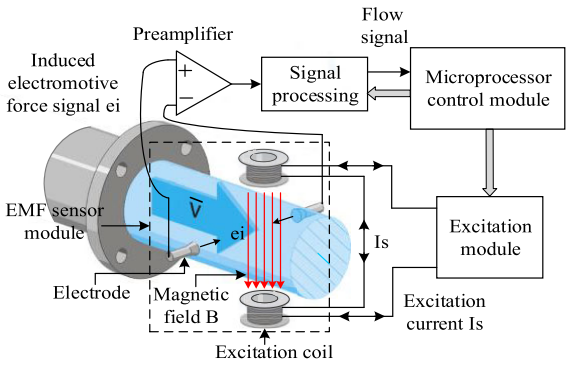

FIGURE 1. Basic structure of an EMF measurement system.

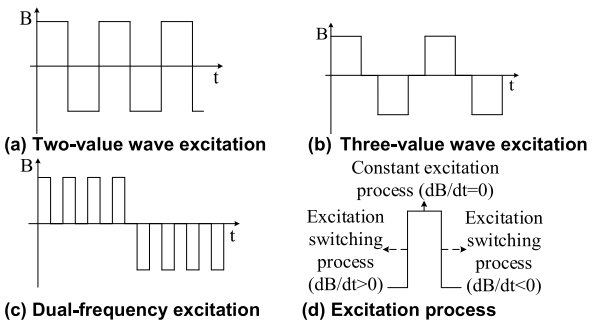

FIGURE 2. Different excitation modes of an EMF.

in Maxwell's equations [17], [18], and its differential form is $\nabla \times E = -\partial B/\partial t$, where $\nabla\times$ is the degree of rotation, $\partial B/\partial t$ is the rate of change of the magnetic field, and E is the vortex electric field. The equation applied to a fixed circuit is equivalent to the "flux rule", which states that the electrodynamic force in a circuit is equal to the rate of change of the magnetic flux through the circuit–which applies whether the flux changes because the field changes or because the circuit moves (or both). The two possibilities–"circuit moves" or "field changes"–are not distinguished in the statement of the rule. However, in the explanation of the rule, two completely distinct laws for the two cases have been used–$v \times B$ for the "circuit moves" [20] and $\nabla \times E = -\partial B/\partial t$ for the "field changes", which correspond to EMF constant excitation process and excitation switching process, respectively.

The principle of EMF measurement in Fig. 1 is to use $v \times B$ of the "circuit moves" during constant excitation to obtain the induced potential proportional to the fluid velocity to measure velocity v. In this paper, the function of $\nabla \times E = -\partial B/\partial t$ in the "field changes" of the EMF excitation switching process will be analyzed to explain the principle that increasing the excitation frequency can enhance the ability to overcome slurry noise. The step excitation method is proposed to give full play to the role of the vortex electric field E in cleaning and rectifying the interference charges on the electrode surface in the process of excitation switching to enhance the ability of an EMF to overcome slurry noise.

According to Faraday's law of electromagnetic induction, during the excitation switching process in Fig. 3 (a), the

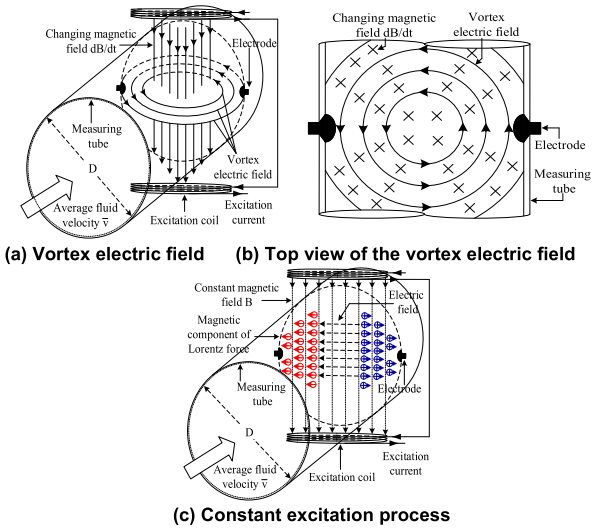

FIGURE 3. Schematic diagram of the two processes of excitation and force on interference charges in an EMF sensor.

rotating vortex electric field is generated by the changing magnetic field *dB/dt* [21]. The vortex electric field has a cleaning ability and can be used to clean and separate charged ions. It is widely used in electrochemistry and biochemistry [22]–[24]. Fig. 3 (b) is the top view of Fig. 3 (a). The direction of the vortex electric field force is tangent to the electrode surface and perpendicular to the charged ions on the electrode's surface. The interference charge will be shifted from the electrode under the effect of the electric field force, and the effect of cleaning the interference charge on the electrode can be achieved.

During the excitation switching process, the larger the *dB/dt* is, the greater the vortex electric field strength. In the case of keeping the same liquid properties, the main way to increase *dB/dt* is to increase the change rate of the excitation current dI_s/dt in the coil. Since the coil is inductive load, high-voltage excitation is often used to increase the rising speed of the excitation current. The constant excitation section uses low voltage excitation to reduce system power consumption.

In the constant excitation after excitation switching, *dB/dt* reaches zero. If the electrode is not affected by solid particle collisions in the measurement time, the signal obtained by the electrode is mainly the induced electromotive force e_i generated by the average fluid velocity $\bar{v}$ under a constant magnetic field B. Additionally, long-term constant excitation will produce polarization charge interference on the electrode. As shown in Fig. 3 (c), the moving charge is affected by the Lorentz force [20]. Positive and negative ions gradually separate and accumulate on both sides of the electrode, forming the electric field. The subsequent ions are subjected to the opposite magnetic force and electric field force and will not deflect when the force is balanced.

Therefore, an EMF commonly uses positive and negative square wave excitation. As shown in Fig. 2, the excitation switching process is on the millisecond level. The magnitude of $\partial B/\partial t$ is much greater than $\bar{v}$, and the vortex electric field force is much larger than the Lorentz force; therefore, the interference charges can be shifted away from the electrode surface. The constant current excitation section is mainly influenced by the Lorentz force. Increasing the excitation frequency increases the excitation switching process; that is, the number of *dB/dt* generations is increased. The smaller the time interval between the two *dB/dt* is, the smaller the probability that the solid particles hit the electrode, and the smaller the probability that the slurry noise interferes with the electrode signal, which helps to overcome slurry noise. For the high concentration slurry fluid, positive and negative square wave excitation with a 160.00 Hz excitation frequency has been used [3], [13]. Moreover, since the induced electromotive force e_i generated by the fluid cutting magnetic induction line is proportional to the excitation intensity, there is always an electromagnetic constant in the positive and negative excitation generated by the excitation current through the excitation coil, so the increase in the excitation frequency is bound to be limited.

Fig. 4 is a photo of the flow measurement system set up. When the fluid velocity is approximately 3 m/s and the sand water mass ratio is 4/125, the flow signals of four different excitation frequencies of three-value rectangular wave excitation are measured, as shown in Fig. 5. The flow signal in the figure contains differential interference [9], [25], [26] in addition to slurry noise. All three-value rectangular wave excitation will result in this kind of peak interference in the switching of excitation. Normally, the constant flow signal is obtained by avoiding the constant positive and negative excitation segments after differential interference. Some nonpeak fluctuations in the flow signal in the figure are the interference caused by the solid particles colliding with the electrode.

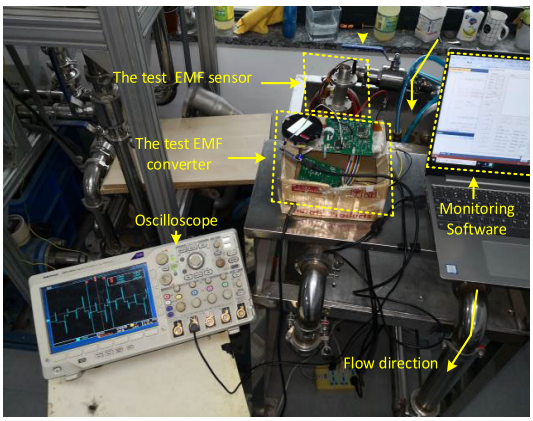

FIGURE 4. Flow measurement experimental system.

When the EMF is used to measure the fluid, during the period after the excitation is switched, the solid particles will collide with the electrode again, causing the signal to generate random interference fluctuations. Fig. 5 (a)-(d) show the waveforms measured at four time scales of 100, 40, 20,

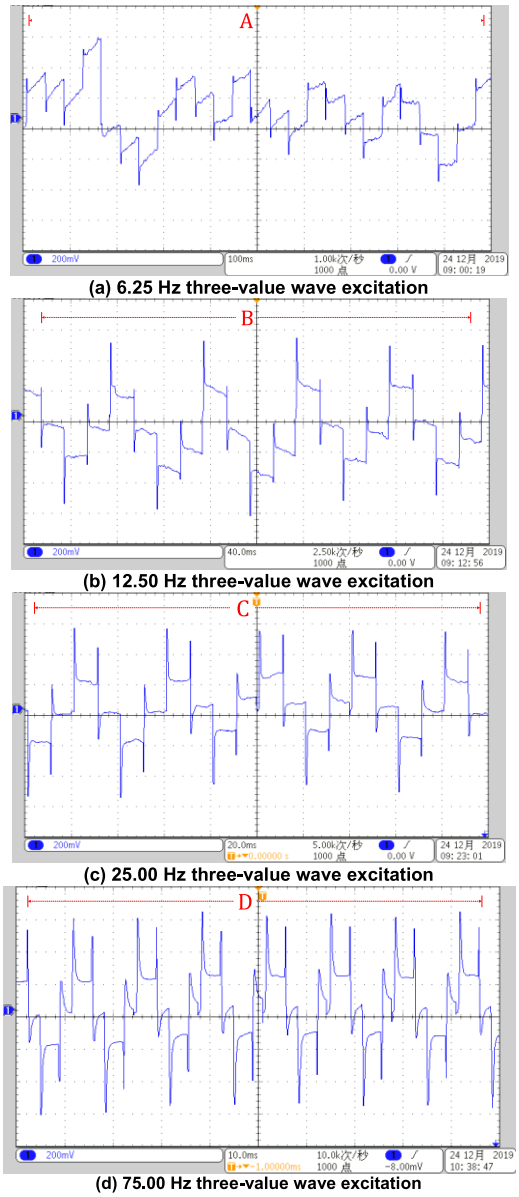

FIGURE 5. Comparison of the flow signal waveforms under different excitation frequencies of three-value wave excitation.

and 10 ms with four excitation frequencies. With the increase in excitation frequency, the time interval between two excitation switching is reduced, and the chance of solid particles colliding with the electrode immediately after switching is smaller. It can be seen that the interference degree of slurry noise is gradually reduced.

Fig. 5 (a) shows the 6.25 Hz flow signal. In measurement section A, the baseline drift of the signal is large. The flow signals corresponding to the three excitation states of positive, zero, and negative excitation are difficult to identify. The signal sampling section after differential interference fluctuates greatly. Fig. 5 (b) shows the 12.50 Hz signal. In measurement segment B, the baseline drift of the flow signal has been reduced, and the corresponding signals of each excitation state are basically recognizable, but the downward fluctuation of the signal sampling section is still very serious. Fig. 5 (c) is the 25.00 Hz signal. The signal sampling section after the differential interference in measurement section C still has a large degree of fluctuation. Fig. 5 (d) is the 75.00 Hz signal. Compared with the first three figures, the amplitude of the baseline drift in measurement section D is small. After the differential interference, the flow signal sampling section is relatively stable. The comparison shows that as the excitation frequency increases, the fluctuation in the flow signal gradually decreases as a whole. This shows that increasing the excitation frequency can enhance an EMF's ability to overcome slurry noise.

III. STEP EXCITATION TECHNOLOGY SOLUTION

A. INTRODUCTION OF STEP EXCITATION TECHNOLOGY

It takes a certain time for the exciting current to rise from 0 to the set value. This time is related to the coil parameters. Due to this limitation, an EMF cannot increase the excitation frequency indefinitely. To increase the magnetic field switching frequency without increasing the overall rise time of the excitation current, this paper proposes step excitation technology. This technology improves the equivalent excitation frequency by splitting the positive (negative) excitation of a three-value rectangular wave in one excitation cycle into two positive (negative) excitations.

In Fig. 6, the three-value rectangular wave excitation current waveform with excitation frequency f_e is shown above, and the excitation current waveform of step excitation after splitting is shown below. The abscissa t is time, and the ordinate I_s is the excitation current. During positive excitation, the direction of the excitation current in the coil is taken as the positive direction. During negative excitation, the excitation current is opposite to the positive excitation direction, and the ordinate is negative. When the excitation current is stable, the ordinates of the excitation current of positive excitation 1, positive excitation 2, negative excitation 1 and negative

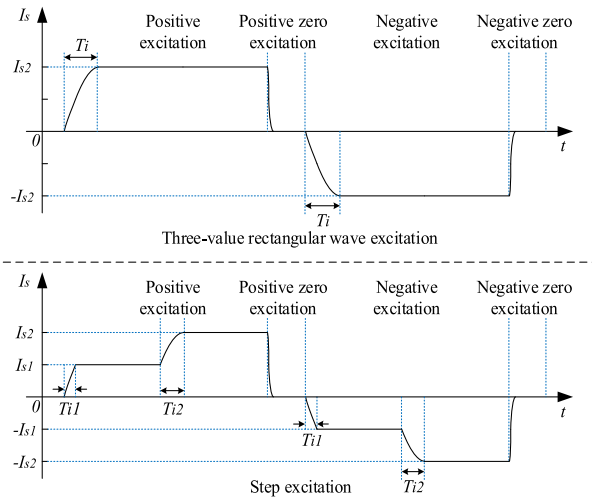

FIGURE 6. Comparison curve of the excitation current between three-value rectangular wave excitation and step excitation.

excitation 2 are I_{s1}, I_{s2}, $-I_{s1}$, and $-I_{s2}$, respectively. In three-value wave excitation, the excitation current rises from 0 to I_{s2} in time T_i. In step excitation, the excitation current rises from 0 to I_{s1} in time T_{i1} and from I_{s1} to I_{s2} in T_{i2}. When the excitation current is stabilized at I_{s1} (or $-I_{s1}$), the stable magnetic field B_1 (or $-B_1$) is generated. When the excitation current is stabilized at I_{s2} (or $-I_{s2}$), magnetic field B_2 (or $-B_2$) is generated.

Assuming that $T_i = T_{i1} + T_{i2}$, the step excitation technology will not increase the total excitation current rise time during positive (negative) excitation, and this ensures that the steady section of the flow signal does not decrease. The step excitation process increases the number of times the excitation current changes, which is equivalent to increasing the excitation frequency to $2f_e$. Here is a simplified model of the excitation system to prove $T_i = T_{i1} + T_{i2}$.

In the simplified model of an excitation system of Fig. 7, E_s is the excitation voltage, R_x is the coil resistance, L_x is the coil inductance, I_s is the excitation current, $\bar{v}$ is the average flow velocity of the fluid, e_i is the induced electromotive force signal, and k_e is the proportional coefficient. The two stages are as follows: the excitation current rises from 0 to the steady state value of I_{s1}, and it rises from I_{s1} to the steady state value of I_{s2}. Both cases belong to the first-order response of an RL series circuit [27].

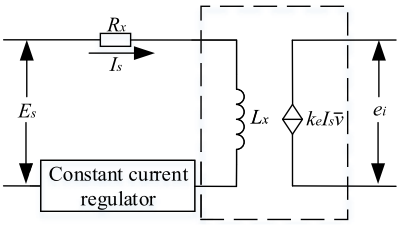

FIGURE 7. Simplified model of an excitation system.

The times for the excitation current to rise from 0 to I_{s1} and from 0 to I_{s2} are T_{i1} and T_i, respectively.

$$T_{i1} = -\tau ln\left(1 - \frac{I_{s1}R_x}{E_s}\right), \quad T_i = -\tau ln\left(1 - \frac{I_{s2}R_x}{E_s}\right) \tag{1}$$

The change in the excitation current from I_{s1} to I_{s2} is the full response of the RL circuit.

$$I_{s2} = I_{s1}e^{-\frac{t}{\tau}} + \frac{E_s}{R_x}\left(1 - e^{-\frac{t}{\tau}}\right), \quad \tau = \frac{L_x}{R_x} \tag{2}$$

The time taken for the excitation current to rise from I_{s1} to I_{s2} is the following:

$$T_{i2} = -\tau ln\left(\frac{I_{s2}R_x - E_s}{I_{s1}R_x - E_s}\right) \tag{3}$$

The sum of the two excitation current rise times of T_{i1} and T_{i2} is the following:

$$\begin{aligned} T_{i1} + T_{i2} &= -\tau ln\left(1 - \frac{I_{s1}R_x}{E_s}\right) - \tau ln\left(\frac{I_{s2}R_x - E_s}{I_{s1}R_x - E_s}\right) \\ &= -\tau ln\left(1 - \frac{I_{s2}R_x}{E_s}\right) \end{aligned} \tag{4}$$

Obviously, $T_i = T_{i1} + T_{i2}$ is true, which means that the equivalent excitation frequency is increased without increasing the rising time of the excitation current.

B. STEP EXCITATION TECHNOLOGY SIGNAL PROCESSING SCHEME

1) TIME-VARYING CURVE OF THE EXCITATION CURRENT AND FLOW SIGNAL VOLTAGE OF STEP EXCITATION

As shown in Fig. 8, Signal 2 describes the time-varying curve of excitation current I_s. The excitation current can be obtained by dividing the sample resistance voltage by the resistance value. Due to the limitation of the page length of the paper, the waveforms at the left and right ends of the oscilloscope in Fig. 8 were appropriately cropped. Signal 1 describes the time-varying curve of the voltage value E of the flow signal. A complete excitation period T includes positive excitation 1 (T_{pm1}), positive excitation 2 (T_{pm2}), positive zero excitation (T_{pz}), negative excitation 1 (T_{nm1}), negative excitation 2 (T_{nm2}), and negative zero excitation (T_{nz}). Normally, $T_{pm1} = T_{pm2} = T_{nm1} = T_{nm2} = T_m$ and $T_{pz} = T_{nz} = T_z$, as shown in (5).

$$T = T_{pm1} + T_{pm2} + T_{nm1} + T_{nm2} + T_{pz} + T_{nz} = 4T_m + 2T_z \tag{5}$$

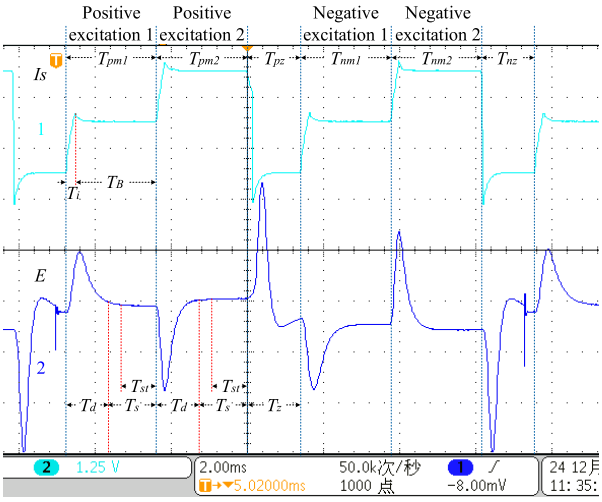

FIGURE 8. Excitation current I_s(up) and flow signal voltage E (down).

For the excitation process, T_i is the excitation current rise time, and T_B is the constant current excitation time. For the generated flow signal, T_d is the establishment time of the flow signal, and T_s is the stable period time of the flow signal.

The equation is as follows:

$$T_m = T_i + T_B = T_d + T_s \tag{6}$$

Obviously, the sampling window T_{st} should be selected within T_s. Additionally, the sampling window should try to avoid the differential interference segment to obtain the flow signal as stable as possible. To ensure the stability of the flow measurement, the sampling window time T_{st} should be greater than 1 ms.

The excitation currents I_{s1} and I_{s2} are 100 mA and 200 mA, respectively. The excitation voltage is 100 V and 30 V in the rising current and constant current excitation stages, respectively. After measuring the EMF sensor, the copper loss resistance $R_x \approx 50\ \Omega$, and the coil inductance $L_x \approx 220$ mH. Step excitation measures the time of each stage of the first step of positive excitation. According to TABLE 1, when the excitation frequencies are similar, for step excitation, $T_i/(T_i + T_B)$ is smaller, and $T_B/(T_i + T_B)$ is larger. It shows that in the excitation signal of step excitation, the proportion of the rise time of the excitation current is smaller, and the proportion of the constant current excitation segment is larger. Additionally, from the measurement data, considering the oscilloscope measurement error, $T_i + T_B = T_d + T_s$ holds.

TABLE 1. Time comparison of each phase between step excitation and three-value rectangular wave excitation.

Excitation mode	Time (ms)	Frequency (Hz) 12.50	25.00	81.25
Step excitation	T_i	0.243	0.262	0.251
	T_B	16.757	7.748	2.109
	T_d	1.333	1.315	1.302
	T_s	15.667	6.665	1.098
	$T_i/(T_i + T_B)$	1.429%	3.271%	10.636%
Three-value rectangular wave excitation	T_i	0.553	0.559	0.547
	T_B	18.417	8.461	3.273
	T_d	1.431	1.492	1.449
	T_s	17.549	7.548	2.391
	$T_i/(T_i + T_B)$	2.915%	6.197%	14.319%

JW Wilson *et al.* proposed pulsed magnetic reluctance (PMR) technology and incorporated it into a dual PMFL/PMR probe. Research shows that the surface and sub-surface defects in ferromagnetic materials can be detected by this technology, which provides a new idea for the processing of EMF induced potential signal in Fig. 8. Next, the theoretical processing scheme of step excitation EMF signal will be introduced.

2) SIGNAL PROCESSING SCHEME FOR STEP EXCITATION

If the excitation current of each step of step excitation is proportional, the magnetic field strength of each step will be proportional; therefore, the induced electromotive force will also have a proportional relationship, and the negative excitation will be the same. Generally, the induced electromotive force may include power frequency interference and zero-drift interference. To overcome the interferences, a flow signal calculation method is introduced below.

The signal sampling is realized by the V/F circuit integrating the flow signal in the sampling window. X_1, X_2, Y_1, and Y_2 are respectively the sampling results of the positive excitation 1, positive excitation 2, negative excitation 1 and negative excitation 2 sampling windows in one cycle. B_1 and B_2 are the magnetic field strengths of the first and second order excitation, respectively. E_1 and E_2 represent the quantized values of the flow signal voltages under the first and second order excitation, respectively. First, Y_1 is subtracted from X_1 to eliminate power frequency interference, and E_1 is calculated. P_1 is the zero drift interference after signal processing, and k_s is the constant coefficient.

$$E_1 = X_1 - Y_1 = 2k_sB_1\bar{v} + P_1 \tag{7}$$

Second, Y_2 is subtracted from X_2 to eliminate power frequency interference, and E_2 is calculated. P_2 is also the zero drift interference after signal processing.

$$E_2 = X_2 - Y_2 = 2k_sB_2\bar{v} + P_2 \tag{8}$$

The DC drift is almost unchanged in one period, and the residual zero drift is approximately equal after the difference calculation. The equation is as follows:

$$P_2 - P_1 \approx 0 \tag{9}$$

Under step excitation, the magnetic field strength has the following relationship:

$$B_2 = 2B_1 \tag{10}$$

When the sampling period is even multiple of the power frequency period, the above equation has eliminated the influence of power frequency interference, the average fluid velocity $\bar{v}$ is as follows:

$$\bar{v} = \frac{E_2 - E_1}{2k_sB_1} \tag{11}$$

The steady and clean flow signals can be obtained by means of sliding average filtering and median filtering of the logarithmic period data, respectively.

3) CALCULATION PROCESS OF THE STEP EXCITATION VELOCITY

The flowing electrolyte cuts the magnetic induction line to generate an induced electromotive force, which is amplified and sampled by V/F integration after baseline correction. To facilitate the unified data processing under various excitation frequencies, 6.25 Hz, 12.50 Hz, 25.00 Hz, 43.75 Hz, and 81.25 Hz are recorded for 1, 2, 4, 7, and 13 cycles respectively; then, $\sum X_1$, $\sum X_2$, $\sum Y_1$, and $\sum Y_2$ are processed. According to (7)-(11), the average induced electromotive force and average fluid velocity can be obtained. The velocity data can be obtained after processing.

In industry, the steady-state fluctuation rate *var* is often used to evaluate the two-phase flow measurement performance of the instrument. This paper also uses *var* to measure

the EMF mortar measurement performance. The calculation method is as shown in (12). *Max*, Min, and Mean are the maximum, minimum, and average flow velocities, respectively. δ_1 is the maximum fluctuation rate, and δ_2 is the minimum fluctuation rate.

$$\begin{cases} \delta_1 = \dfrac{Max - Mean}{Mean} * 100\% \\ \delta_2 = \dfrac{Min - Mean}{Mean} * 100\%, \end{cases} \quad var = \frac{\delta_1 - \delta_2}{2} \tag{12}$$

C. PARAMETER DESIGN OF THE EXCITATION CURRENT

The selection of the excitation current is a common problem faced by all EMF designers and major manufacturers. The selection of the upper and lower limits of the excitation current is restricted by many factors, which makes it a comprehensive optimization problem. The following analysis will be carried out from the perspectives of sensitivity, the sensor coil, excitation system power consumption, hardware design and so on.

1) INFLUENCING FACTORS OF THE MINIMUM EXCITATION CURRENT

a: FROM THE PERSPECTIVE OF SENSITIVITY

The sensitivity of an EMF sensor is expressed as the value of the induced electromotive force generated per unit flow rate. The sensitivity of the early AC excitation mode meter is 1 to 1.5 mV/(m/s), and the low-frequency rectangular wave excitation is 0.2 to 0.4 mV/(m/s) at the beginning. Now, the sensitivity of the typical EMF should be at least 0.15 to 0.2 mV/(m/s) [28]. To ensure the measurement of the low fluid velocity, the excitation current should not be too low; otherwise, the sensitivity of the sensor will decrease, the signal-to-noise ratio of the induced signal will decrease, and the accuracy will deteriorate [29]. When the excitation current is 100 mA, the sensitivity of a step excitation EMF is approximately 0.55 mV/(m/s), and the sensitivity value satisfies the design index.

b: FROM THE PERSPECTIVE OF THE SENSOR COIL

If the excitation current is too low, more coil turns are needed to maintain the same magnetic field strength, which will increase the size of the sensor and reduce the coil efficiency. The coil inductance value is directly proportional to the square of the number of turns of the coil [30]. Increasing the number of turns will cause the inductance to rise rapidly. It can be seen from (1) that this will increase the rise time of the excitation current, thereby reducing the steady-state measurement time, which is disadvantageous to the realization of high-frequency excitation.

Therefore, according to the EMF industry optimization for many years, the excitation current is generally not less than 100 mA [31].

2) INFLUENCING FACTORS OF THE MAXIMUM EXCITATION CURRENT

a: ANALYSIS FROM THE PERSPECTIVE OF THE EXCITATION SYSTEM POWER CONSUMPTION AND HARDWARE DESIGN

The power consumption of an early EMF is high, and the typical power consumption range is 10 to 100 W. Now, the power consumption can be reduced to 0.5 W [32]. According to Table 2, when the step excitation voltage is 30 V and the excitation current is 100 mA/200 mA, the coil power consumption is low. If the excitation current is greater than 300 mA, the coil power consumption will be greatly increased. The excitation system needs a constant current shunt circuit for shunt and heat dissipation. One constant current shunt shall be opened for 100 mA excitation, with three constant current diodes in total; and two constant current shunts shall be opened for 200 mA excitation, with six constant current diodes in total. By analogy, the greater the excitation current is, the greater the demand for constant current diodes. Therefore, it is not a cost-effective hardware design to use an excitation current of more than 200 mA.

b: FROM THE PERSPECTIVE OF THE COIL

Increasing the excitation current will increase the coil power consumption. Although the number of turns of the excitation coil can be reduced, it is necessary to select a coil having a larger copper wire cross-sectional area and a stronger current carrying capacity, which may lead to a heavy structure and serious heating of the sensor.

Generally, due to the above perspectives, the EMF industry generally uses an excitation current that is less than 250 mA.

3) SUMMARY OF THE EXCITATION CURRENT SELECTION METHOD

The EMF industry regards 100 mA to 250 mA as the common excitation current selection range. For example, Germany Siemens uses a 125 mA excitation current [33], Japan Yokogawa uses a 250 mA excitation current [34], Switzerland ABB uses a 180 mA excitation current [35], Zhejiang Diyuan uses a 125 mA or a 250 mA excitation current [36], etc. According to the excitation current of the EMFs of each company, the excitation current of the step excitation is set from 100 mA to 250 mA. To facilitate the calculation and analysis, when the excitation step number is 2, I_{s1} and I_{s2} are set as 100 mA and 200 mA, respectively.

D. PARAMETER DESIGN OF THE EXCITATION STEP ORDER

The magnetic field is changed during the excitation switching phase. Due to the electrode wiring deviation and other reasons, an EMF will experience the ''transformer effect'' and form differential interference [9], [25], [26] in the measurement circuit. The duration of the differential interference is related to the coil parameters, electrode wiring and other factors. In an excitation cycle, every time the excitation current is switched, one differential interference will be generated, which will reduce the signal sampling time after avoiding the

differential interference. Therefore, the step number of step excitation should not be too large, and it needs to be carefully optimized. The following factors should be considered in step number optimization.

From the perspective of the excitation current, the excitation current needs to be accurately divided with the number of steps. When the step number is higher than 2, it is difficult to keep the excitation current of each step in the optimal selection range. From the perspective of the hardware, in order to achieve higher step excitation current switching, a constant current switching control circuit, a constant current shunt and so on need to be added, which will increase the hardware power consumption and costs. From the perspective of the excitation frequency, the larger the step number is, the larger the proportion of differential interference, and the smaller the sampling window T_{st}.

From the perspective of easy implementation, the step excitation scheme currently uses two steps.

E. EXCITATION FREQUENCY

When selecting the excitation frequency of the step excitation, the first consideration is to overcome the power frequency interference [37]. The effect of power frequency interference can be eliminated by keeping the sampling windows during positive and negative excitation in the same phase, and subtracting the negative excitation sampling results from the positive excitation sampling results.

Due to the inductive load characteristics of the excitation coil, the domestic EMF excitation frequency generally does not exceed approximately 12.50 Hz. EMF products from abroad such as Japan have 75.00 Hz and 160.00 Hz frequencies. To adapt to different measurement requirements and facilitate the comparison experiments, the step excitation frequency is set as 6.25 Hz, 12.50 Hz, 25.00 Hz, 43.75 Hz, and 81.25 Hz.

F. EXCITATION VOLTAGE

Step excitation adopts the high-low voltage switching excitation method. Thus, 100 V high-voltage excitation is used in the excitation current rising stage, and 30 V low-voltage excitation is used in the excitation magnetic field stabilization stage. High voltage (100 V) excitation can reduce the excitation current rise time, and low voltage (30 V) excitation can reduce the system power consumption.

1) EXCITATION VOLTAGE AMPLITUDE CALCULATION

Then the excitation voltage amplitude will be analyzed, the paper selects the EMF sensor produced by Zhejiang Diyuan Instrument Co., Ltd. The diameter range is DN10-DN200. The measured copper loss resistance R_x is 50Ω, and the coil inductance L_x is 220 mH. The high-voltage power supply E_s should satisfy the following equations.

$$E_s > \frac{I_{s1}R_x}{1-e^{-\frac{R_xT_i}{L_x}}} * 100\%, \quad E_s > \frac{I_{s2}R_x - I_{s1}R_xe^{-\frac{R_xT_i}{L_x}}}{1-e^{-\frac{R_xT_i}{L_x}}} * 100\% \tag{13}$$

The sampling window is required to be not less than 1 ms at 81.25 Hz. Considering the differential interference and other factors, the rise time of the excitation current should not be less than 0.3 ms. Equation (13) shows that the high-voltage power supply should be greater than 75.86 V. Considering the voltage drop of the H-bridge switch tube and the constant current module, 100 V was selected as the high voltage power supply. On the other hand, when the excitation current reaches the 200 mA steady state, the voltage drop on the excitation coil is 22 V. Considering the voltage drop and power consumption of each module, the low voltage power supply is set to 30 V.

2) RISE TIME AND ADJUSTMENT TIME OF THE EXCITATION CURRENT

This paper considers that solving the rise time of the excitation current is a classical first-order step response problem. In general, the theoretical calculations and implementations are very consistent.

In this paper, the problem of the constant current adjustment speed of excitation has been considered in the system design. High-frequency electronic components are used in constant current circuits. A constant current circuit is mainly composed of an MOS tube and an operational amplifier [38]. The MOSFET switching tube is an FQT4N20L, and the constant current circuit adjustment operational amplifier is an OPA2335. The turn-on rise time t_r of the MOS tube is 70ns, and the turn-off fall time t_f is 40ns [39]. Therefore, the MOS tube adjustment time is less than 100 ns. The gain-bandwidth product (GBW) of the operational amplifier is 2.00 MHz, and the output voltage slew rate (SR) is 1.6 V/μs [40]. The OPA2335's power supply voltage is +5 V, and so its maximum output time when adjusting and comparing is less than 3.125 μs. It can be observed that in the constant current circuit adjustment time brought by the excitation voltage switching, the main part of the excitation current rise time is the theoretically calculated inductive load step response time. The paper will analyze the rising and adjustment process of the excitation current from the following three aspects.

a: EFFECT OF THE EXCITATION VOLTAGE ON THE EXCITATION CURRENT RISING CURVE

According to (1), the excitation current rise time is affected by the excitation voltage E_s and the excitation current steady-state value I_s. After determining the copper loss resistance R_x, the coil inductance L_x and the steady-state value I_s of the excitation current, the main parameter affecting the rise time of the excitation current is the high-voltage excitation voltage E_s. The rise curve of the excitation current under different excitation voltages is shown in the following picture.

The solid blue, red, and yellow solid lines in Fig. 9 are the rising current curves of the excitation current at excitation voltages of 30 V, 65 V, and 100 V, respectively. It can be seen that since the coil is inductive load, the higher the excitation voltage is, the faster the excitation current rises. When the excitation voltage is 30 V and the excitation frequency is

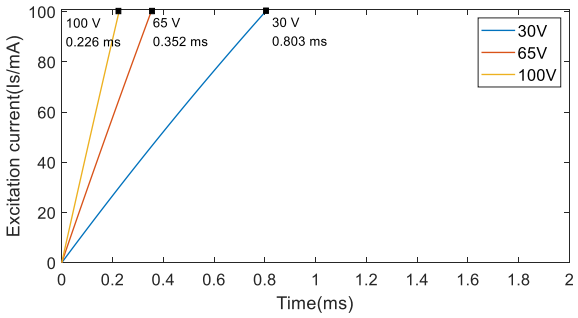

FIGURE 9. Excitation current rising curve under different voltages.

6.25 Hz, 25.00 Hz, and 81.25 Hz, the proportion of the excitation current rise time to the constant current excitation time is approximately 2.25%, 10.38%, and 28.11%, respectively, and it is reduced to 0.63%, 2.92%, and 10.72%, respectively, at 100 V.

b: EXCITATION CURRENT RISE TIME

First, the theoretical calculation of the rise time of the excitation current is performed. The rise time of the zero to first-step excitation current is T_{i1}, and the rise time of the first- to second-step excitation current is T_{i2}. Both processes belong to the first-order response of an RL series circuit [27]. The actual nominal value of the excitation coil inductance L_x is 220 mH, and the actual nominal value of the coil resistance R_x is 50 Ω. I_{s1} is 100 mA, and I_{s2} is 200 mA. Substituting these into (1) and (3) of section 3.1 of the paper, the theoretical values are the following: $T_{i1} = 225.69\ \mu$s, and $T_{i2} = 237.90\ \mu$s.

As shown in Fig. 10, the rise time of zero to the first-step excitation current T_{i1} is approximately 243 μs, and the rise time of the first to second-step excitation current T_{i2} is approximately 219 μs. The relative error between the measured value and the theoretical calculation value of T_{i1} is 7.67%, and the relative error between the measured value and the theoretical calculation value of T_{i2} is 7.94%.

Equation (14) can calculate the magnetic field change rate $d\Phi/dt$. k_B is a small coefficient, N is the number of coil turns, dI_s/dt is the change rate of the exciting current, and S is the cross-sectional area of the pipeline, which can be calculated using the sensor diameter of 40 mm. From the measured data, the rising slope dI_s/dt is 411.52A/s at $0 \rightarrow 100$ mA, and the rising slope is 456.62A/s at $100 \rightarrow 200$ mA. The change rate of $d\Phi/dt$ is proportional to the change rate of dI_s/dt, and the scale factor is k_BSN. Moreover, the rise time of the excitation current is very short, and dI_s/dt approaches infinity; therefore, $d\Phi/dt$ also approaches infinity. The induced vortex electric field is very strong; thus, the interfering ions on the electrodes can be cleaned during the excitation switching stage.

$$\frac{d\Phi}{dt} = S\frac{dB}{dt} = S\frac{d(k_B I_s N)}{dt} = k_B SN\frac{dI_s}{dt} \tag{14}$$

c: OSCILLOGRAPH MEASUREMENT RESULTS OF THE EXCITATION CURRENT ADJUSTMENT PROCESS

In the actual system, the excitation current is controlled by the voltage feedback of the 12.5 Ω resistor in the excitation current loop. Fig. 11 (a) shows the sample resistance voltage waveform when the zero excitation changes to the first-step excitation at the 81.25 Hz excitation frequency. Fig. 11 (b) shows the voltage waveform of the sampling resistance when the first-step excitation changes to the second-step excitation.

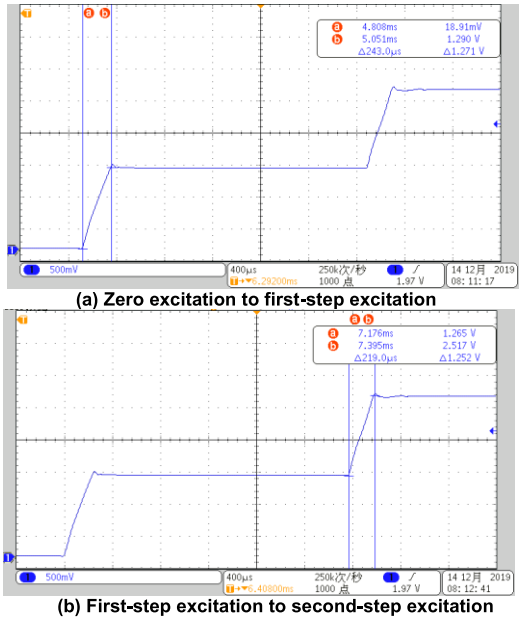

FIGURE 10. Screenshot of the oscilloscope waveform during the excitation current rise.

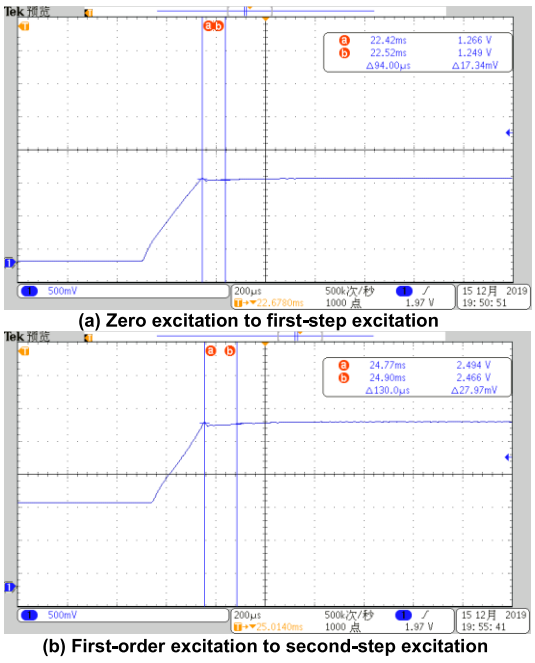

FIGURE 11. Oscillograph waveform of excitation current under step excitation.

The constant current excitation section of the second half of each waveform provides a data sampling section with a duration of 1 ms.

3) EFFECT OF THE EXCITATION VOLTAGE ON POWER CONSUMPTION

The power consumption of an excitation system is approximately the sum of the power P_c of the excitation coil and the power of the excitation constant current regulator P_i, which satisfies equations (15) and (16). Considering the excitation voltages of 30 V and 100 V, the power of the sensor when the excitation field is stable is shown in TABLE 2. In the table, I_s is the excitation current, E_s is the excitation voltage, P_{total} is the total power, P_c is the excitation coil power, and P_i is the constant current regulator power.

$$P_{total} = P_c + P_i = E_s I_s \tag{15}$$

$$P_c = I_s^2 R_x \tag{16}$$

TABLE 2. Power consumption of the excitation stable section under different excitation voltages and excitation currents.

I_s(mA)	E_s(V)	P_{total}(W)	P_c(W)	P_i(W)	P_c/P_{total}
100	30	3	0.95	2.05	31.67%
	100	10		9.05	9.50%
200	30	6	3.80	2.20	63.33%
	100	20		16.20	19.00%

As the excitation voltage increase, the power of the constant current regulator will increase. For excitation currents of 100 mA and 200 mA, if the excitation voltage always stays at 100 V, approximately 90.5% and 81% of the power is dissipated in the constant current regulator circuit when the magnetic field is stable, respectively. This will affect the stable operation of the circuit. Therefore, the step excitation EMF adopts the excitation control scheme of high and low voltage switching.

IV. DESIGN OF STEP EXCITATION SYSTEM

A. HARDWARE DESIGN SCHEME

Based on the step excitation design parameters, the system hardware design was carried out. As shown in Fig. 12, the system hardware includes a power module, a microprocessor control module, an excitation module, a signal processing module, a human machine interface module, a storage module and an output module. The excitation module generates the step excitation current under the control of the microprocessor control module, the excitation current generates the magnetic field in the excitation coil, the conductive fluid cuts the magnetic line and generates the induced electromotive force, and the induced electromotive force is processed by the preamplifier and the signal processing circuit to obtain the flow signal.

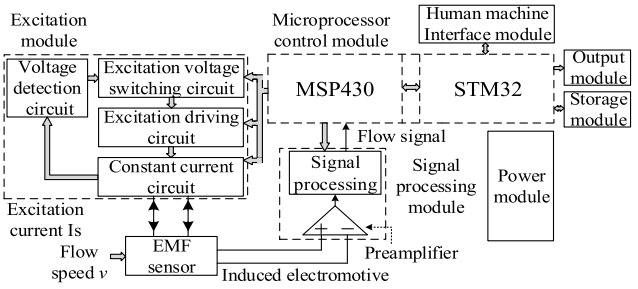

FIGURE 12. Step excitation magnetic flowmeter system scheme.

1) EXCITATION MODULE DESIGN

The excitation voltage switching circuit is used to achieve 100 V high-voltage excitation during excitation switching process and 30 V low-voltage excitation during the constant excitation process to ensure that the excitation current rise time and system power consumption meet the requirements.

The excitation driving circuit uses the NMOS excitation driving circuit based on a pulse transformer. Four NMOS tubes constitute an H bridge switching circuit, which is used to control the direction of the excitation current in the excitation coil and realize positive and negative excitation.

A constant current circuit is used to realize constant current excitation and the switching excitation current. A constant current circuit composed of an operational amplifier and MOSFET is used to maintain the stability of the excitation current and establish a stable magnetic field. A shunt circuit composed of several constant current diodes is used to improve the performance of the constant current circuit. This circuit is also responsible for switching between different excitation currents.

The voltage detection circuit is used to detect the magnitude of the excitation current, realize the hardware switching of the high and low voltage power supply, and ensure the safety of the system together with the microprocessor control module.

2) SIGNAL PROCESSING MODULE

The signal processing module mainly includes the preamplifier and the subsequent signal processing circuits. The preamplifier based on differential amplifications can realize functions such as high impedance conversion, the suppression of common mode interference, and the amplification of weak flow signals.

The subsequent signal processing circuit can perform baseline negative feedback adjustment on the flow signal during the zero excitation phase to ensure the stability of the flow signal reference, and then the signal is amplified and processed without distortion.

The amplified signal needs to be converted into frequency or digital information by an analog-to-digital conversion circuit to be processed by the microprocessor. A step excitation EMF adopts V/F conversion to collect data to improve the anti-interference performance.

B. SOFTWARE SCHEME DESIGN

1) OVERALL PLAN INTRODUCTION

This system uses two microprocessor chips. The secondary controller MSP430F5529 is responsible for controlling the excitation timing, collecting the flow signal and preprocessing. The main controller STM32F103C8T6 further processes, displays, and outputs the flow signal transmitted by the secondary controller and realizes the human-computer interaction function. The task division of the two processors is shown in Fig. 13.

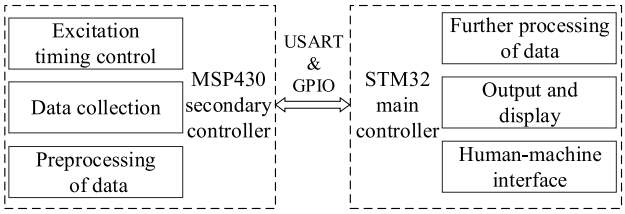

FIGURE 13. Dual controller task division diagram.

2) MAIN CONTROLLER SOFTWARE FUNCTION

The main controller software workflow is shown in Fig. 14 (a). The initialization module completes the initialization of the hardware device, system clock and system parameters and realizes the synchronization function with the secondary controller.

The main controller realizes human-computer interaction through an LCD and buttons. The LCD displays the flow data and assists users in modifying the relevant parameters by pressing the button. The communication module is responsible for driving the 4-20 mA analog current output circuit, the frequency output circuit and the internal USART module to communicate with other devices in the industrial control field. The memory chip is used to save the system parameters required during system startup, such as the excitation frequency, high-voltage time, and damping time.

3) SECONDARY CONTROLLER SOFTWARE FUNCTION

The secondary controller software workflow is shown in Fig. 14 (b). The initialization module is used to set initialization state after the system is powered on to ensure that the software and hardware are ready, and the MSP430 will perform a handshake operation with the STM32 to complete the synchronization between two controllers. The high- and low-voltage power switching module is used to cooperate with excitation timing control module to control the accurate switching of the excitation power from 100 V to 30 V.

According to the excitation sequence, the excitation sequence control module controls the periodic switching states of the four MOSFETs in the H-bridge switching circuit to realize the step change of the excitation current. The excitation timing sequence is generated by the timing interruption of the 16-bit timer of the microprocessor. The baseline adjustment control module controls the baseline adjuster in

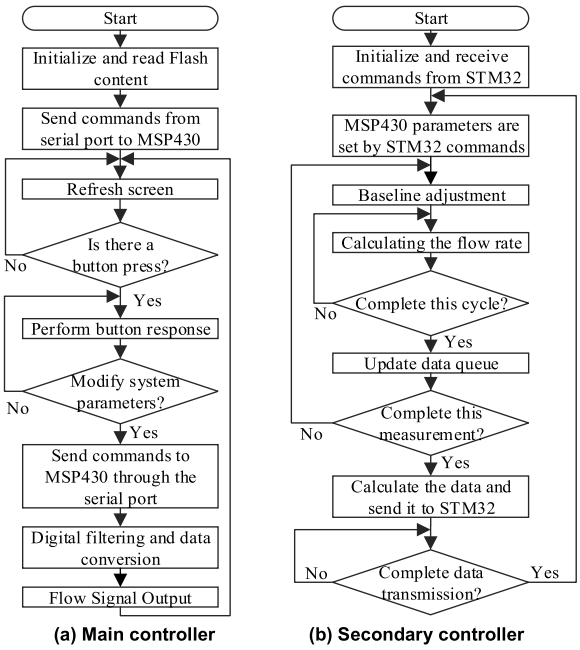

FIGURE 14. Software flow chart of the main controller and secondary controller.

the feedback signal amplification processing module. At the end of each cycle, the signal reference voltage is adjusted to stabilize the preset voltage value. The communication module is mainly used for accepting the commands of the main controller; setting the parameters such as the EMF working mode, the excitation frequency according to the command; and periodically transmitting the preprocessed flow data to the main controller.

V. CONTRAST EXPERIMENT OF THE STEP EXCITATION EMF AND THE THREE-VALUE RECTANGULAR WAVE EXCITATION EMF BASED ON WAVELET TRANSFORM SIGNAL PROCESSING

For the traditional three-value rectangular wave excitation EMF with an excitation frequency of 25.00 Hz, the flow signal can be processed by a software algorithm to improve the ability of the EMF to overcome slurry noise. In reference [6], a nonstationary noise and periodic signal separation method based on the stationary wavelet transform is proposed, and this paper uses the method of reference [6] to analyze the mortar flow signal under three-value rectangular wave excitation.

A. DECOMPOSITION SCALE DETERMINATION AND DETAIL COEFFICIENTS AT EACH SCALE

The signal sampling frequency is 2500.00 Hz, and the excitation frequency is 25.00 Hz. According to reference [6], the maximum scale of the wavelet coefficients with a 25.00 Hz fundamental frequency signal components is six, and the optimal decomposition scale is 7. The Haar wavelet is used as the basis function to decompose and reconstruct the EMF output signal.

Based on the Haar function, the detail coefficients d_1 to d_7 and approximate coefficient c_7 can be obtained by SWT wavelet decomposition [41], [42]. The detail coefficients d_1 to d_7 reflect the high-frequency characteristics of the original signal, which is mainly composed of the zero mean periodic signal and the high-frequency component of the slurry noise. The approximate coefficient c_7 reflects the low-frequency characteristics of the original signal and is mainly composed of the low-frequency drift portion of the slurry noise and the random disturbance. The slurry noise belongs to 1/f noise, which mainly concentrates in d_7 and c_7. The abrupt slurry noise will cause the detail coefficients and the approximate coefficient to be distorted.

Fig. 15 shows the variation curves of detail coefficients d_1 and d_7 with time T. The analysis shows that d_1 fluctuates at approximately 0 V; d_7 is more severely affected by low frequency slurry noise, showing obvious aperiodic jump.

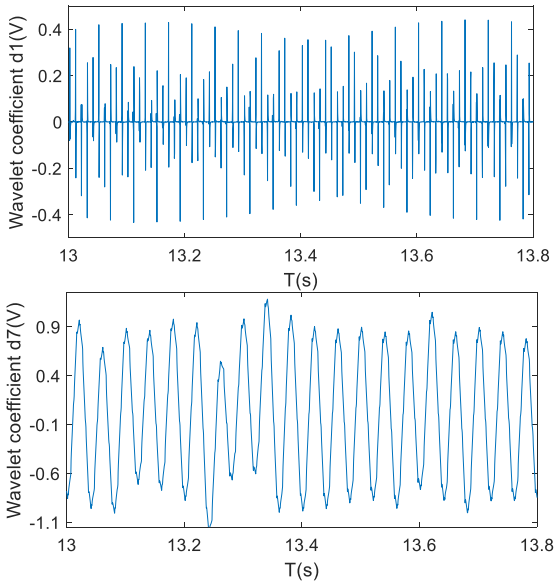

FIGURE 15. Detail coefficients d_1 (top) and d_7 (bottom).

B. DETAIL COEFFICIENTS d_1 TO d_7 AND APPROXIMATE COEFFICIENT c_7 FILTERING

d_1 to d_7 were extracted according to phase s ($1 \leq s \leq T$), and the same phase sequence $u_{j,s}$ ($1 \leq j \leq 7$) of each scale was obtained. T is the number of points for each cycle, and T is 100 at 25.00 Hz excitation. First, the nonlinear median filter with sliding window W and mean window M is used to remove the impulse noise, and then the sliding average filter with window N is applied to remove the white noise. Parameter $W = 50$, $M = 10$, and $N = 50$. The filtered data d_1 to d_7 can be obtained by interpolating and restoring the same-phase sequence of each scale according to the original phase relation. After filtering, the detail coefficients have stronger periodicity, and the influence of slurry noise is greatly weakened.

Because of the spectrum leakage, the approximate coefficient c_7 still contains part of the 25.00 Hz signal component and 75.00 Hz and 125.00 Hz harmonic components. Therefore, three frequency notches of 25.00 Hz, 75.00 Hz, and 125.00 Hz are performed on c_7, and the trap widths are all 1.00 Hz. Then, the c_7 signal component obtained by the notch is also subjected to the same phase sequence decomposition and filtering.

Fig. 16 (a) and Fig. 16 (b) are the comparison curves of c_7 before and after filtering, time T is the abscissa, and the range is 13 to 15 s. From the time domain, c_7 exhibits non-periodic fluctuations before filtering, and exhibits significant periodicity after filtering. Fig. 16 (c) and Fig. 16 (d) show the spectrum of c_7 before and after filtering. From the frequency

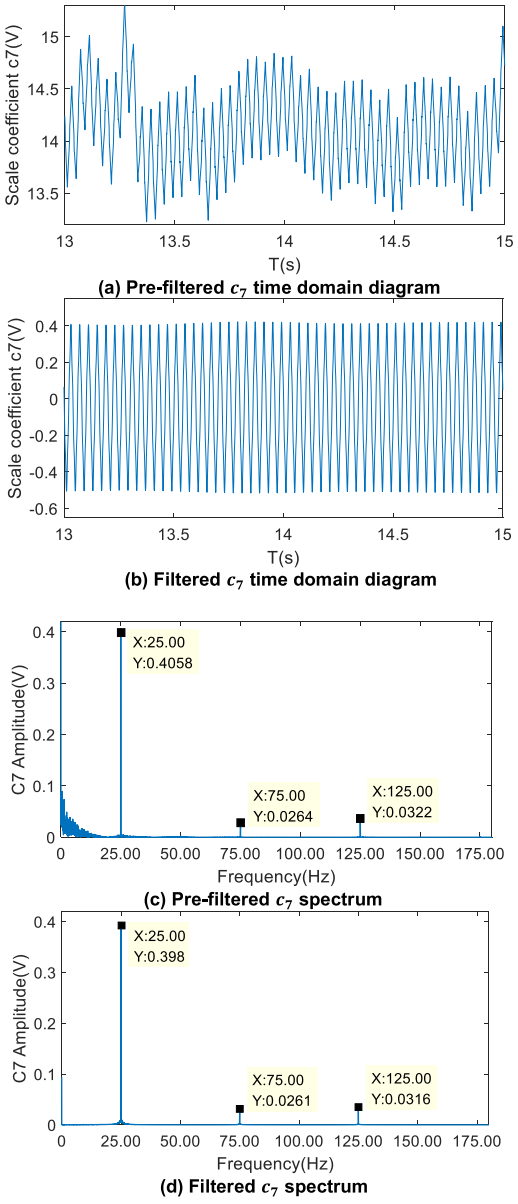

FIGURE 16. Time-domain graph and spectrum of the approximate coefficients before and after filtering.

domain, c_7 contains many low-frequency noise components before filtering. After filtering, the low-frequency noise component is effectively stripped while the 25.00 Hz flow signal component and 75.00 Hz and 125.00 Hz harmonic components are retained.

C. INVERSE WAVELET TRANSFORM AND SIGNAL AMPLITUDE RECONSTRUCTION

Detail coefficients d_1 to d_7 and approximate coefficient c_7 can reconstruct the filtered flow signal according to the ISWT inverse wavelet transform. As shown in Fig. 17, the above figure shows the filtered flow signal, and the figure below shows the slurry noise signal. It can be seen that the flow signal is periodic, and the slurry noise signal has obvious aperiodicity and randomness.

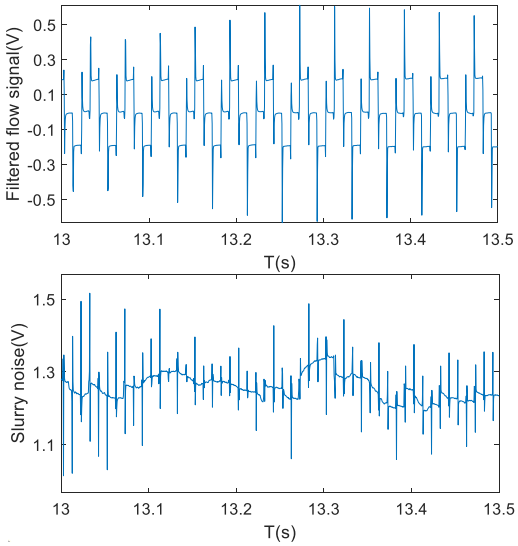

FIGURE 17. Filtered flow signal (top) and slurry noise signal (bottom).

Then, the amplitude of the filtered flow signal is demodulated, and the amplitude demodulation method is shown in (17):

$$flow\,(h) = 1/n * \sum_{i=1}^{n} \frac{D_{h-1}\,(i) - D_h\,(i)}{2} \tag{17}$$

D_{h-1} and D_h are the sampling data of positive excitation and negative excitation in the h-th cycle, respectively, each containing n data (n is 25). To avoid the differential interference, the last 10 of every 25 data are calculated and modulated, and the *flow* is the amplitude demodulation result.

Fig. 18 is the comparison of the amplitude demodulation results of the original signal and the filtered signal. The abscissa time T ranges from 0 to 36 s, and ordinate is the demodulated signal amplitude. The red dotted line is the original signal, and the blue solid line is the filtered signal. It can be seen from the figure that the signal processing method based on the stationary wavelet transform obtains a relatively stable and smooth flow signal.

D. COMPARISON OF THE EXPERIMENTAL RESULTS OF THE STEP EXCITATION EMF AND THE THREE-VALUE RECTANGULAR WAVE EXCITATION WAVELET METHOD

The paper uses the steady-state fluctuation rate (*var*) to evaluate the application effect of the wavelet transform signal processing method on mortar signals. When the mass ratio of sand to water is 8/125 and the excitation frequency is 25.00 Hz, three-value rectangular wave excitation and step excitation are used to measure data at the flow rates of approximately 1 m/s, 2 m/s, and 3 m/s, respectively. The measurement results are shown in TABLE 3. Num represents the experiment number.

TABLE 3. Comparison of the volatility between three-value rectangular wave excitation and step excitation.

Num	Three-value wave excitation wavelet scheme			Step excitation		
	Max (m/s)	Min (m/s)	*var* (%)	*Max* (m/s)	Min (m/s)	*var* (%)
1	1.014	0.985	1.455	0.994	0.989	0.292
2	1.011	0.985	1.324	0.993	0.987	0.288
3	1.014	0.989	1.241	0.994	0.987	0.318
1	2.117	1.906	5.301	2.014	2.001	0.312
2	2.158	1.829	8.214	2.010	1.998	0.275
3	2.035	1.744	7.291	2.012	1.996	0.389
1	3.532	2.662	14.507	2.992	2.961	0.516
2	3.408	2.685	12.050	2.986	2.956	0.500
3	3.305	2.527	12.964	2.983	2.950	0.552

As shown in Fig. 18, the stationary wavelet transform is a very effective signal processing algorithm to overcome slurry noise [6]. Meanwhile, the step excitation scheme based on increasing the equivalent excitation frequency is also an effective method to improve the ability to overcome slurry noise. The following sections will compare the two methods. It can be seen from the table that when the mass ratio of sand to water is 8/125, the overall signal volatility of the wavelet processing method is less than 14.507%, and the volatility at 1 m/s, 2 m/s, and 3 m/s is less than 1.455%, 8.214%, and 14.507%, respectively. When using a 25.00 Hz step excitation, the overall volatility of the flow signal is less than 0.552%, and the volatility is less than 0.318%, 0.389%, and 0.552% at 1 m/s, 2 m/s, and 3 m/s, respectively.

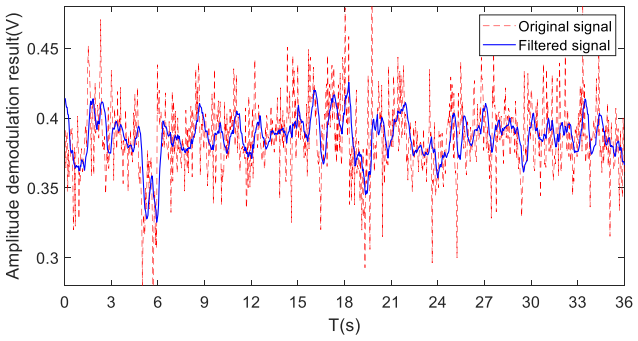

FIGURE 18. Comparison of the amplitude demodulation results of the original signal and the filtered signal.

The EMF fluctuation rate based on the step excitation at each flow rate is smaller than that based on the three-value rectangular wave excitation EMF.

In addition, it should be noted that the application range of the three-value rectangular wave excitation signal processing method based on the wavelet transform method is limited. If it is replaced by other types of slurry, such as mine slurry, paper slurry or coal water slurry, the characteristics of the slurry noise may change, and the effect of the algorithm may no longer be stable. Moreover, the wavelet transform method also puts forward certain requirements on the EMF excitation frequency, which limits its application in more occasions. Correspondingly, step excitation EMF improves the excitation scheme, which improves the equivalent excitation frequency without increasing the rise time of the excitation current, and enhances the ability of an EMF to overcome slurry noise. According to the data of TABLE 3, when the excitation frequency is 25.00 Hz in the mortar measuring environment with the sand-to-water mass ratio of 8/125, the steady-state fluctuation rate of EMF based on step excitation is generally lower than that based on the three-value rectangular wave excitation at the velocity of 1 m/s, 2 m/s and 3 m/s. The signal processing method of the step excitation EMF is simpler and more applicable.

VI. COMPARATIVE EXPERIMENT BETWEEN THE STEP EXCITATION EMF AND THE YOKOGAWA AXF 040G EMF

A. EXPERIMENTAL DEVICE INTRODUCTION

To thoroughly analyze the performance of the step excitation EMF at different measurement environments, the paper uses the flow measurement experimental device shown in Fig. 19 to collect data. The device uses the AXF 040G EMF with an excitation frequency of 160.00 Hz to set the fluid velocity and serves as the reference flowmeter. The experimental flowmeter is a step excitation EMF, which uses a sensor with a diameter of DN40. In the experiment, the mortar is made of quartz sand and water. The grain size of quartz sand is 20 to 120 mesh. The oscilloscope's sampling frequency is set to 2500.00 Hz, and sampling time is set to 40 s.

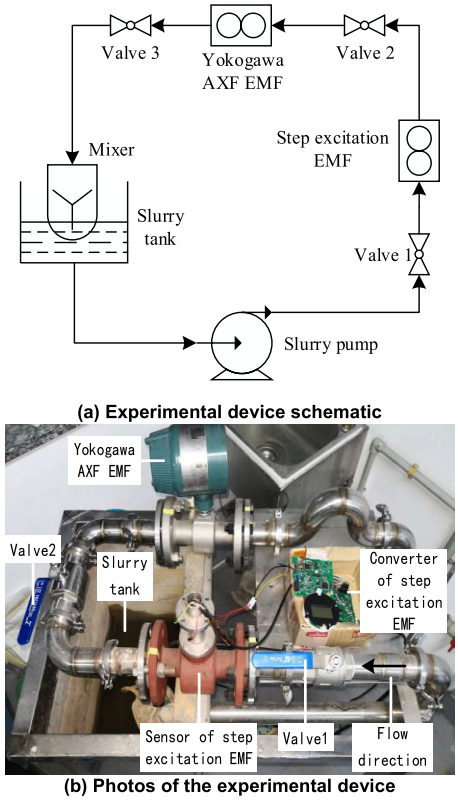

FIGURE 19. EMF flow measurement experimental device.

FIGURE 20. Photos of the flowmeter calibration site.

B. CALIBRATION EXPERIMENT

According to the National Metrological Verification Regulations (JJG 1033-2007), in the flow calibration laboratory of Zhejiang Diyuan Instrument Co., Ltd., the static volume method calibration device is used to calibrate the clean water volume flow of the developed EMF, as shown in Fig. 20. The calibration device in the picture is composed of the flowmeter under test, a standard container, a water pump, and several pipes and valves. The diameter of the pipe used for calibration is 100 mm.

In the experiment, the EMF uses pulse output. At the beginning of the calibration, the control device starts to count the EMF's output pulses. After the calibration, the total pulse count is multiplied by the single pulse equivalent to obtain the total volume of the EMF measured. Then, the relative indication error can be obtained by comparing the data with the total volume measured by the standard device. The flow value obtained by this calibration method is reliable and accurate. As a method of establishing the standard flow, it is widely used in the calibration of many flowmeters. The experiment calibrates three flow points of $11m^3/h$, $82m^3/h$, and $168m^3/h$. Each flow point is tested 3 times to obtain repeatability index. The experimental results are shown in TABLE 4.

To evaluate the performance of the developed EMF measurement system, the measurement results are processed and analyzed according to the verification procedures.

(1) The relative indication error of the single calibration of each flow point of the flowmeter is calculated according to equation (18). During the j-th calibration of the i-th flow point, E_{ij} is the relative indication error of the tested flowmeter, Q_{ij} is the accumulated flow value of the tested flowmeter,

TABLE 4. Calibration data of developed EMF in clean water environment.

Flow points (m^3/h)	Pulse number	Test EMF volume (L)	Standard volume (L)	Verification time (s)	Relative indication error (%)
11.454	65572	803.31	803.19	252.453	0.015
11.499	65679	804.62	805.94	252.312	-0.163
11.481	65667	804.48	804.88	252.388	-0.050
82.402	63716	780.58	780.03	34.078	0.070
82.171	65192	798.66	797.11	34.922	0.195
82.690	64403	788.99	788.86	34.344	0.016
168.706	328637	4026.09	4025.08	85.891	0.025
168.802	328368	4022.79	4025.88	85.859	-0.077
168.974	327475	4011.85	4013.12	85.500	-0.032

and $(Q_s)_{ij}$ is the accumulated flow value of the calibration device.

$$E_{ij} = \frac{Q_{ij} - (Q_s)_{ij}}{(Q_s)_{ij}} * 100\% \tag{18}$$

(2) The relative indication error E_i of the flowmeter under test at the i-th verification point is calculated according to equation (19), and n is the number of calibrations for the i-th flow point.

$$E_i = \frac{1}{n} \sum_{j=1}^{n} E_{ij} \tag{19}$$

(3) The repeatability of the i-th flow point of the flowmeter $(E_r)_i$ is calculated according to equation (20):

$$(E_r)_i = \sqrt{\frac{1}{n-1} \sum_{j=1}^{n} \left(E_{ij} - E_i\right)^2} \tag{20}$$

TABLE 4 is the calibration results of the developed EMF. According to equation (20), the repeatability of the developed EMF at three flow points of $11m^3/h$, $82m^3/h$, and $168m^3/h$ are calculated to be 0.090%, 0.092%, and 0.051%, respectively, which is less than 0.1% repeatability required by the accuracy of class 0.3 instruments. The maximum error is 0.195%, which is less than the 0.3% error required by class 0.3 instruments. Both the repeatability and error meet the accuracy requirements of class 0.3 instruments.

Next, the linearity index will be analyzed in the manuscript. In the EMF calibration experiment, the output pulse frequency P of the EMF is proportional to the average fluid velocity $\bar{v}$, which satisfies equation (21). In EMF industry, K is defined as gain. Affected by factors such as production process in actual production, EMF may exhibit zero drift, that is, the output pulse frequency b at zero fluid velocity is not zero. The coefficient K and b values can be obtained from calibration experiment, and then coefficient correction can be performed in the software algorithm.

$$P = K * \bar{v} + b \tag{21}$$

The calibration experiment calibrates three flow points in total, and each flow point is tested 3 times. For each calibration result, average fluid velocity $\bar{v}$ can be calculated based on standard volume, verification time, and diameter of the pipe. According to the pulse number and verification time, the output pulse frequency P of the tested EMF can be calculated. According to data in Table 4, the relationship curve between P and $\bar{v}$ can be calculated, as shown in Fig. 21. The fitting results show that $K \approx 640.908$, $b \approx 0.754$. The results show that there is a good linear relationship between the output pulse frequency P and the average fluid velocity $\bar{v}$ of the detected EMF. In Fig. 21, the degree index R squared of linear fitting of linear trend can be calculated as 0.9999. The high degree index indicates that the EMF under test has good linear characteristics and high stability.

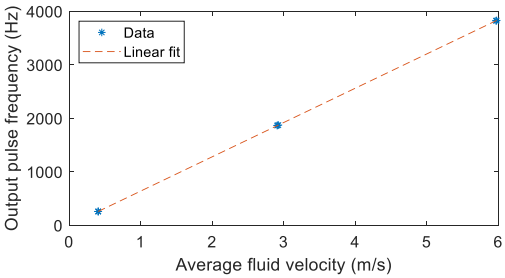

FIGURE 21. The linear characteristics of the EMF.

C. CLEAN WATER MEASUREMENT EXPERIMENT

Achieving the accurate and stable measurement of the clean water flow is one of the basic requirements of an EMF. In this paper, the control experiment of the clear water measurement is carried out using the device of Fig. 19. During the experiment, the parameters such as the damping coefficient of the instrument are set to increase the stability of the measurement results. Five velocity points of 1 m/s, 1.5 m/s, 2 m/s, 2.5 m/s, and 3 m/s are selected for the experiment. The Yokogawa AXF 040G EMF is used as the standard flowmeter, and the valve is adjusted to make the flow rate fluctuate around the flow point. The flow rates of the measured flowmeter and the comparison flowmeter are counted for a period of time at the excitation frequencies of 6.25 Hz, 25.00 Hz, and 81.25 Hz, respectively. The experimental results are shown in TABLE 5. Num in the table represents the experiment number.

According to TABLE 5, the error bars shown in Fig. 22 can be drawn. The error bars are calculated using the standard deviation. The horizontal axis in the figure is the experiment number Num in the table, and the vertical axis is the steady-state fluctuation rate. According to the analysis of TABLE 5 and Fig. 22, the performances of the step excitation EMF and Yokogawa AXF 040G EMF are equivalent in the measurement of clean water, and the steady-state fluctuation rate of measurement results is generally kept within 0.500%.

D. MORTAR MEASUREMENT EXPERIMENT

To further verify the performance of the step excitation EMF, a comparative experiment of the step excitation EMF and Yokogawa AXF 040G EMF is carried out. The sand-to-water

TABLE 5. Clean water measurement steady state fluctuation experiment.

Frequ -ency (Hz)	Num	Step excitation EMF			Yokogawa AXF EMF		
		Max (m/s)	Min (m/s)	*var* (%)	*Max* (m/s)	Min (m/s)	*var* (%)
6.25	1	1.006	0.998	0.387	1.004	0.999	0.250
	2	1.507	1.497	0.327	1.506	1.498	0.267
	3	2.010	1.996	0.361	2.001	1.993	0.200
	4	2.513	2.492	0.423	2.507	2.492	0.300
	5	3.003	2.987	0.259	3.010	2.998	0.200
25.00	6	1.005	0.997	0.413	1.004	1.002	0.100
	7	1.507	1.494	0.431	1.505	1.496	0.300
	8	2.009	1.993	0.400	2.004	1.991	0.325
	9	2.509	2.490	0.372	2.505	2.494	0.220
	10	3.011	2.985	0.431	3.012	2.982	0.500
81.25	11	0.995	0.991	0.192	1.005	1.002	0.150
	12	1.512	1.505	0.237	1.504	1.494	0.333
	13	2.008	1.997	0.285	2.001	1.996	0.125
	14	2.509	2.500	0.181	2.508	2.493	0.300
	15	2.999	2.988	0.183	3.011	2.992	0.317

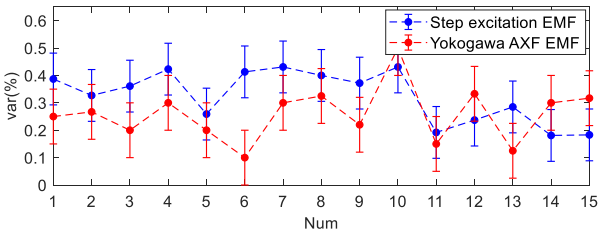

FIGURE 22. Graphical analysis of TABLE 5.

TABLE 6. Mortar steady state fluctuation comparison experiment - excitation frequency 6.25 Hz.

Ratio	Num	Step excitation EMF			Yokogawa AXF EMF		
		Max (m/s)	Min (m/s)	*var* (%)	*Max* (m/s)	Min (m/s)	*var* (%)
1/125	1	0.998	0.990	0.367	1.014	1.003	0.550
	2	2.017	2.006	0.259	2.015	1.991	0.600
	3	3.006	2.914	1.548	3.049	2.992	0.950
2/125	4	1.010	1.002	0.408	1.008	0.986	1.100
	5	1.999	1.967	0.804	2.012	1.986	0.650
	6	3.049	2.967	1.359	3.038	2.958	1.333
4/125	7	1.007	0.998	0.417	1.015	1.003	0.600
	8	2.004	1.984	0.485	2.015	1.974	1.025
	9	3.078	2.938	2.318	3.057	2.971	1.433
8/125	10	0.999	0.992	0.372	1.015	0.994	1.050
	11	2.030	1.986	1.095	2.010	1.962	1.200
	12	3.060	2.902	2.631	3.072	2.948	2.067

mass ratios of the mortar are 1/125, 2/125, 4/125, and 8/125, respectively. The step excitation frequency is set to 6.25 Hz, 25.00 Hz, and 81.25 Hz. In the table, Ratio represents the mass ratio of sand to water in the mortar. When the readings of the Yokogawa's AXF 040G EMF fluctuate up and down in the range of 1 m/s, 2 m/s, and 3 m/s, PC software is used to collect the experimental data and compare the steady-state volatility of the two instruments in different experimental environments. TABLE 6 to TABLE 8 show the summarized experimental data. Num in the tables represents the experiment number.

TABLE 7. Mortar steady state fluctuation comparison experiment - excitation frequency 25.00 Hz.

Ratio	Num	Step excitation EMF			Yokogawa AXF EMF		
		Max (m/s)	Min (m/s)	*var* (%)	*Max* (m/s)	Min (m/s)	*var* (%)
1/125	1	1.003	0.995	0.402	1.011	0.998	0.650
	2	2.039	2.014	0.622	2.019	1.992	0.675
	3	3.013	2.959	0.915	3.053	2.972	1.350
2/125	4	1.005	0.996	0.451	1.010	0.996	0.700
	5	2.003	1.979	0.614	2.014	1.984	0.750
	6	3.043	2.991	0.874	3.036	2.953	1.383
4/125	7	1.005	0.995	0.500	1.014	1.001	0.650
	8	1.997	1.988	0.246	2.016	1.966	1.250
	9	3.021	2.995	0.429	3.061	2.963	1.633
8/125	10	0.993	0.987	0.293	1.014	0.993	1.050
	11	2.012	1.996	0.395	2.013	1.957	1.400
	12	3.001	2.950	0.862	3.069	2.959	1.833

TABLE 8. Mortar steady state fluctuation comparison experiment - excitation frequency 81.25 Hz.

Ratio	Num	Step excitation EMF			Yokogawa AXF EMF		
		Max (m/s)	Min (m/s)	*var* (%)	*Max* (m/s)	Min (m/s)	*var* (%)
1/125	1	0.998	0.994	0.183	1.012	1.001	0.550
	2	2.006	1.996	0.252	2.016	1.984	0.800
	3	2.996	2.979	0.272	3.045	2.986	0.983
2/125	4	0.998	0.993	0.240	1.008	0.995	0.650
	5	2.013	2.004	0.214	2.013	1.985	0.700
	6	3.005	2.987	0.296	3.045	2.964	1.350
4/125	7	1.005	0.996	0.453	1.015	0.998	0.850
	8	2.007	1.994	0.322	2.016	1.971	1.125
	9	3.020	2.986	0.564	3.063	2.969	1.567
8/125	10	0.985	0.977	0.382	1.010	0.986	1.200
	11	2.028	2.018	0.243	2.012	1.959	1.325
	12	2.996	2.973	0.398	3.068	2.947	2.017

To visually show the steady-state fluctuation rate change trend of the step excitation EMF and the Yokogawa AXF EMF in different measurement environments, the following error bar graph is also used for analysis. According to TABLE 6-TABLE 7, Fig. 23-Fig. 25 are drawn, respectively.

From the data in the table, when the sand-to-water mass ratio of the mortar is 8/125, the steady-state fluctuation rate(*var*) measured by the step excitation EMF is less than 2.631%, 0.862%, and 0.398% at 6.25 Hz, 25.00 Hz, and 81.25 Hz excitation frequencies, respectively. The overall *var* of Yokogawa AXF 040G EMF is less than 2.067%. Combined with Figs. 23-25, it can be concluded that for step excitation EMF, the *var* at the excitation frequency of 6.25 Hz is slightly higher than that of the Yokogawa EMF, the *var* at excitation frequency of 25.00 Hz is slightly lower than that of the Yokogawa EMF, and the *var* at excitation frequency of 81.25 Hz is significantly lower than that of the Yokogawa EMF. The results show that the mortar measurement performance of the step excitation EMF during low frequency excitation is slightly weaker than that of the Yokogawa EMF. When the excitation frequency is higher than 25.00 Hz,

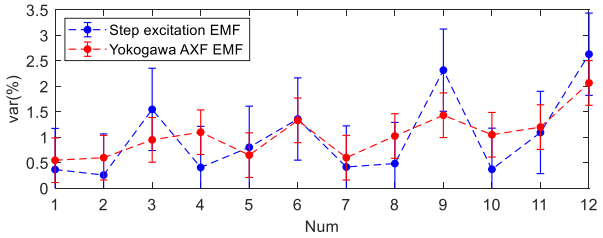

FIGURE 23. Graphical analysis of TABLE 6.

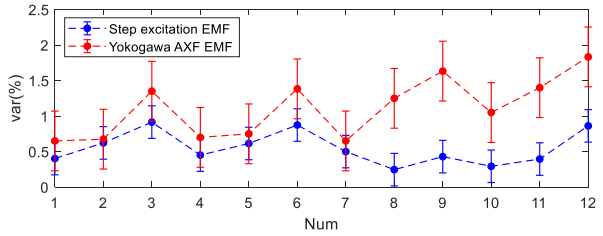

FIGURE 24. Graphical analysis of TABLE 7.

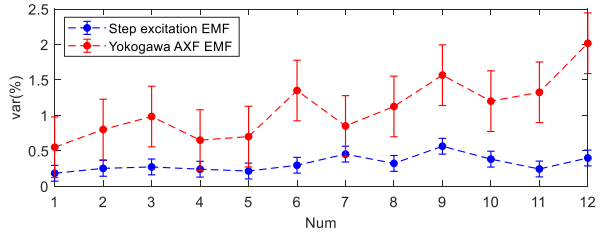

FIGURE 25. Graphical analysis of TABLE 8.

the mortar measurement performance is better than that of the Yokogawa EMF.

When the sand-to-water mass ratio of the mortar is 1/125, 2/125, 4/125, and 8/125, the equivalent excitation frequency of the step EMF of the 81.25 Hz excitation frequency is 162.50Hz, and its steady-state fluctuation rates are less than 0.272%, 0.296%, 0.564%, and 0.398%, respectively. Additionally, the fluctuation rates of the Yokogawa EMF with a 160.00 Hz excitation frequency are less than 1.350%, 1.383%, 1.633%, and 2.067%, respectively. Under similar excitation frequencies, the step excitation EMF has better flow measurement stability at various concentrations. Combined with Fig. 25, it can be concluded that when the excitation frequencies are similar, the step excitation EMF generally has a low steady-state fluctuation rate at various concentrations.

E. DYNAMIC RESPONSE EXPERIMENT

The dynamic response experiment is a supplement to the above experiment. The purpose of the experiment is to verify that the two flowmeters are performing clean water and mortar measurement experiments at similar dynamic response speeds. The dynamic response speed mainly refers to the rapid response ability of the flowmeter when the flow in the pipeline changes. In the experiment, the parameters of the two instruments stay unchanged.

For the mortar with the sand-to-water ratio of 4/125, the fluid velocity is set to 0, then the flow switch is opened to the maximum within 1 s to make the fluid velocity rise to the maximum value rapidly. When the fluid velocity is stable, the flow switch is closed within 1 s so that fluid velocity decreases to 0. Record the dynamic response time of the two flowmeters, see TABLE 9:

TABLE 9. Mortar measurement dynamic response speed comparison experiment.

Velocity variation (m/s)	Step excitation frequency (Hz)	Step excitation EMF(s)	Yokogawa AXF EMF (s)
0→3	6.25	20.481	19.823
	25.00	19.366	21.461
	81.25	22.723	25.526
3→0	6.25	20.802	23.063
	25.00	22.885	24.285
	81.25	20.163	22.867

The response speed of EMF in practical industrial applications is related to its filtering algorithm and damping coefficient. Since the specific software algorithm and parameters of the AXF 040G EMF software are not disclosed to the public, two instruments can only be evaluated simply by their macroscopic performance. When fluid velocity changes by approximately 3 m/s, the volume flow changes by approximately 13.56 m^3/h. It can be seen from table that response times of two flowmeters under this environment are within 26 s. This verifies that two flowmeters are performing clean water and mortar measurement experiments at similar dynamic response speeds.

VII. CONCLUSION

The main contents of this paper are summarized as follows:

(1) From the perspective of Maxwell's equations and the vortex electric field, by analyzing the two processes of square wave excitation, the paper shows that *dB/dt* can generate a vortex electric field during the excitation switching process, which can shift away the interference charge of the electrode. The paper confirmed that increasing the excitation frequency can increase the number of *dB/dt* generated per unit of time, thereby improving the EMF's ability to overcome slurry noise. The paper also provides the actual measurement waveforms. The inductive load of the excitation coil is also analyzed in this paper. The existence of the rise time of the excitation current limits the increase of the excitation frequency. To solve the above contradiction, this paper proposes the step excitation scheme.

(2) From the perspective of theoretical calculations, it is shown that the step excitation scheme can divide the rise time of the original excitation current into two step excitation processes. It is concluded that the step excitation can increase the number of *dB/dt* generated without increasing the rise

time of the excitation current, which improves the ability to overcome slurry noise at the equivalent excitation frequency.

(3) From the perspective of the parameter design, the paper analyzes the excitation current, the excitation step, and the excitation voltage suitable for step excitation, and implements the hardware.

(4) From the experimental perspective, the contrast experiment of the step excitation EMF and the three-value rectangular wave excitation EMF based on stationary wavelet transform signal processing was performed. The experiments show that the step excitation EMF has a lower fluctuation rate when measuring mortar.

(5) From the perspective of the experiments, the step excitation EMF calibration experiment is conducted to verify its performance; and the comparative analysis of the clean water measurement, the mortar measurement and the dynamic responses of the step excitation EMF and Yokogawa AXF 040G EMF are performed. The experiments verify that the step excitation EMF has the ability to enhance the resistance to slurry noise at the same excitation frequency.

(6) The step excitation EMF can be applied to flow measurement in clean water and mortar environments, enhance the ability of an EMF to overcome slurry noise, and promote the development of the field of flow measurement in industrial and agricultural production.

There is still room for further research in the optimization of the system parameters of the step excitation EMF and the calculation and processing of the multiple sets of flow signals using the step excitation EMF.

REFERENCES

[1] L. Ge, H. Li, Q. Huang, G. Tian, G. Wei, Z. Hu, and J. Ahmed, "Electromagnetic flow detection technology based on correlation theory," *IEEE Access*, vol. 8, pp. 56203–56213, 2020.

[2] H. Eren and J. Goh, "Signal extraction from magnetic flowmeters for density measurements," in *Proc. Conf. 10th Anniversary. IMTC/ Adv. Technol. I M. IEEE Instrum. Meas. Technolgy Conf.*, May 1994, pp. 1213–1216.

[3] Y. Aoyama and A. Yasumatsu, "ADMAG AXR two-wire magnetic flowmeter," *Yokogawa Tech. Rep. English Ed.*, vol. 53, no. 2, pp. 79–84, 2010.

[4] E. Eryurek, R. Gao, and T. Lh, "High accuracy signal processing for magnetic flowmeter," U.S. Patent 6 505 517 B1, Jan. 14, 2003.

[5] M. A. Linnert, S. O. Mariager, S. J. Rupitsch, and R. Lerch, "Dynamic offset correction of electromagnetic flowmeters," *IEEE Trans. Instrum. Meas.*, vol. 68, no. 5, pp. 1284–1293, May 2019.

[6] L.-P. Liang, K.-J. Xu, and W. Xu, "SWT based separation method for periodic signal with non-stationary noise and its application in EMF," *Flow Meas. Instrum.*, vol. 42, pp. 78–88, Apr. 2015.

[7] A. Sophian, G. Y. Tian, D. Taylor, and J. Rudlin, "A feature extraction technique based on principal component analysis for pulsed Eddy current NDT," *NDT E Int.*, vol. 36, no. 1, pp. 37–41, 2003.

[8] N. Dubovikova, Y. Kolesnikov, and C. Karcher, "Experimental study of an electromagnetic flow meter for liquid metals based on torque measurement during pumping process," *Meas. Sci. Technol.*, vol. 26, no. 11, Nov. 2015, Art. no. 115304.

[9] W. C. Cai, Z. Y. Ma, and G. F. Qu, (in chinese). *Electromagnetic Flowmeter*. Beijing, China: China Petrochemical Press, 2004.

[10] I. Wada, "Electromagnetic flowmeter utilizing magnetic fields of a plurality frequencies," U.S. Patent 5 090 250 A, Feb. 25, 1992.

[11] *FSM4000-The Electromagnetic Flowmeter of Choice For Critical Applications in a Wide Range of Industries*. Zürich, Switzerland: ABB Instrumentation, 2010.

[12] G. Livelli, "New magmeter combines benefits of AC and DC technologies," *Pulp Paper*, vol. 82, no. 3, pp. 40–44, 2008.

[13] O. Yoshikawa, N. Shikuya, T. Tanaka, S. Tanabe, T. Arai, and H. Ohta, "New ADMAG AXF series magnetic flowmeters," *Yokogawa Tech. Rep.-English Ed.*, no. 37, pp. 15–20, 2004.

[14] H. Song, H. Dong, Z. Yuan, J. Zhu, H. Zhang, and Y. Huang, "An EEMD-based electromagnetic induction method for nondestructive testing of buried metal conductors," *IEEE Access*, vol. 7, pp. 142261–142271, 2019.

[15] L. Wang and A. M. Al-Jumaily, "Imaging of lung structure using holographic electromagnetic induction," *IEEE Access*, vol. 5, pp. 20313–20318, 2017.

[16] D. Kong, Z. Shuai, W. Li, and D. Wang, "Electromagnetic vibration characteristics analysis of a squirrel-cage induction motor under different loading conditions," *IEEE Access*, vol. 7, pp. 173240–173248, 2019.

[17] J. C. Maxwell, "A dynamical theory of the electromagnetic field," *Philos. Trans. Roy. Soc. London*, vol. 155, pp. 459–512, Dec. 1865.

[18] A. Anees and L. Angermann, "Time domain finite element method for Maxwell's equations," *IEEE Access*, vol. 7, pp. 63852–63867, 2019.

[19] M. N. O. Sadiku, *Elements of Electromagnetics*, 4th ed. Oxford U.K.: Oxford Univ. Press. 2007, p. 386.

[20] R. P. Feynman, R. B. Leighton, and M. L. Sands, "The Feynman lectures on physics," *Amer. J. Phys.*, vol. 3, no. 9, p. 1, 1963.

[21] L. T. Chow, *Electromagnetic Theory*. Sudbury, MA, USA: Jones Bartlett. 2006, ch 5, p. 171.

[22] T. B. Jones, *Electromechanics of Particles*. New York, NY, USA: Cambridge Univ. Press, 1995.

[23] A. D. Goater, *AC Electrokinetic Bioassays Development of Electrorotation Assay for Analytes in Water*. Bangor, Wales: Univ. Wales Bangor, 1999.

[24] Y, Huang, R, Hölzel, R, Pethig, X B, Wang, "Differences in the AC electrodynamics of viable and non-viable yeast cells determined through combined dielectrophoresis and electrorotation studies," *Phys. Med. Biol.*, vol. 37, no. 7, p. 1499, 1992.

[25] A. Michalski, J. Jakubowski, and Z. Watral, "The problems of pulse excitation in electromagnetic flowmeters [instrumentationnotes]," *IEEE Instrum. Meas. Mag.*, vol. 16, no. 5, pp. 47–52, Oct. 2013.

[26] K. Saito, Y. Sakurai, and T. Okayama, "Study on stabilized zero-point of electromagnetic flowmeter with rapid excitation," in *Proc. Conf.10th Anniversary. IMTC/ Adv. Technol. I M. IEEE Instrum. Meas. Technolgy Conf.*, May 1994, pp. 829–832.

[27] A. H. Panuluh and A. Damanik, "Lagrangian for RLC circuits using analogy with the classical mechanics concepts," *J. Phys., Conf. Ser.*, vol. 909, Nov. 2017, Art. no. 012005.

[28] *Analog Devices, Inc*. Accessed: Aug. 15, 2019. [Online]. Available: https://www.analog.com/en/analog-dialogue/articles/electromagnetic-flow-meters-achieve-high-accuracy.html [OL]

[29] J. A. Shercliff, *The Theory of Electromagnetic Flowmeasurement*. Cambridge, U.K.: Cambridge Univ. Press, 1962.

[30] M. Sarul, G. Yıldırmaz, and R. Gülgün, "Measurement of the inductance of a coil with core at different currents by a dc chopper," *Elect. Eng.*, vol. 82, pp. 273–277, Aug. 2000.

[31] B. L. Tian, "The dynamic response and zero-point stability of the electromagnetic flowmeter," (in chinese), *Process Autom. Instrum.*, vol. 12, no. 9, pp. 14–18, 1991.

[32] B. Rc, *Flow Measurement Handbook*. Cambridge, U.K.: Cambridge Univ. Press, 2000.

[33] Siemens. *SITRANS F M MAGFLO Electromagnetic Flowmeter*. Accessed: Sep. 10, 2018. [Online]. Available: www.siemens.com/flow

[34] K. Kuromori and S. Goto, "Advanced magnetic flow meter with dual frequency excitation," (in Japanese), *Yokogawa Tech. Rep.*, vol. 32, no. 3, pp. 13–18, 1988.

[35] ABB. *Electromagnetic Flowmeter*. Accessed: Sep. 22, 2018. [Online]. Available: https://new.abb.com/products/measurement-products/flow/electromagnetic-flowmeters/process-industry/processmaster-fep300

[36] *Zhejiang Diyuan Instrument Co., Ltd*. (Oct. 1, 2015). *YYD Electromagnetic Flowmeter Use's Manual*. Accessed: Sep. 18, 2018. [Online]. Available: http://www.zjdiyuan.com/product/detailed-2.htm

[37] A. S. Vale-Cardoso and H. N. Guimarães, "The effect of 50/60 hz notch filter application on human and rat ECG recordings," *Physiolog. Meas.*, vol. 31, no. 1, pp. 45–58, Jan. 2010.

[38] P. Horowitz, W. Hill, and R. J. Rollefson, "The art of electronics," *Amer. J. Phys.*, vol. 58, no. 7, pp. 238–260, Jul. 1990.

[39] *200V Logic N-Channel Mosfet*, FQT4N20L datasheet, Fairchild Semiconductor Corporation, Sunnyvale, CA, USA, May 2001.

[40] *0.05μV/°C max, Single-Supply COMS Operational Amplifiers Zero-Drift Series*, OPA2335 datasheet, Texas Instruments, Dallas, TX, USA, Jun. 2002.

[41] A. Patra and S. Saha Ray, "Two-dimensional Haar wavelet collocation method for the solution of stationary neutron transport equation in a homogeneous isotropic medium," *Ann. Nucl. Energy*, vol. 70, pp. 30–35, Aug. 2014.
[42] C. Yi, Y. Lv, H. Xiao, T. Huang, and G. You, "Multisensor signal denoising based on matching synchrosqueezing wavelet transform for mechanical fault condition assessment," *Meas. Sci. Technol.*, vol. 29, no. 4, Apr. 2018, Art. no. 045104.

BIN LI received the B.S. degree in computer science and the M.S. degree in automation from the Shanghai University of Science and Technology, Shanghai, China, in 1982 and 1988, respectively. He is currently a Professor with the School of Mechanical and Electrical Engineering and Automation, Shanghai University, Shanghai. He has authored or coauthored over 17 refereed articles. He holds 19 patents. His current research interests include electromagnetic flowmeters, vortex flowmeters, ultrasonic flowmeters, sparse signal processing, and calibration instruments.

YUE YAN received the B.S. degree in automation from Nantong University, Nantong, China, in 2017. He is currently pursuing the M.S. degree in detection technology and automation devices from Shanghai University, Shanghai, China. His current research interest includes electromagnetic flowmeters.

JIE CHEN received the B.S. degree in automatic control, the M.S. degree in detection technology and automatic equipment, and the Ph.D. degree in control theory and control engineering from Shanghai University, Shanghai, China, in 2002, 2005, and 2010, respectively. She is currently a Lecturer with the School of Mechanical and Electrical Engineering and Automation, Shanghai University. She has authored or coauthored over 31 articles in journals and conferences. Her current research interests include electromagnetic flowmeters and sparse signal processing.

XINGHANG FAN, photograph and biography not available at the time of publication.